Channel-capture mechanism in low-energy neutron capture by ^{12}C

Yu-Kun Ho*
Centre of Theoretical Physics, China Centre of Advanced Science and Technology (World Laboratory), Beijing, China and Nuclear Science Department, Fudan University, Shanghai, China

H. Kitazawa and M. Igashira
Research Laboratory for Nuclear Reactors, Tokyo Institute of Technology, O-okayama, Meguro-ku, Tokyo, Japan
(Received 1 April 1991)

This paper shows that, in the neutron energy region from thermal to 30 keV, the measured neutron radiative capture cross sections of ^{12}C feeding the first four bound states in ^{13}C can be well understood in the framework of a channel-capture model for the $E1$ transition. The characteristics for each kind of transition are investigated.

Recently, Nagai and his collaborators [1] reported an interesting measurement on neutron radiative capture cross sections of ^{12}C at 30 keV. The results are summarized in Table I, along with the previously published thermal neutron capture cross sections [2], as well as relevant data. One distinguished feature of those results is that the capture cross sections for either thermal or 30-keV neutrons are very small. Also, as for the branching ratio, the chief transition at thermal energy is the transition feeding the ground state in ^{13}C, but at 30 keV it is the first excited-state transition. A previous paper [4] indicated that the thermal neutron capture data for ^{12}C can be attributed to the channel-capture contribution which is of a strong destructive interference between the potential-scattering wave and the resonance-scattering wave. The measured total capture cross section at 30 keV is 16.8 ± 2.1 μb. Using the published resonance parameters of all levels above and below the neutron binding energy, the total compound-nucleus capture cross section at 30 keV is obtained to be 0.26 μb, far from accounting for the measured data. It is therefore of interest to investigate this problem on the base of the channel-capture model, to explore the physical significance and characteristics of the mechanisms underlying the transitions, and to examine the difference between the transitions at thermal energy and 30 keV.

The channel-capture model [5,6] assumes that the gamma-ray emission is accompanied by a single-particle transition from a scattering state of partial wave (l,j)

$$U_{lj}^{+J}(r)=\mathrm{Re}\langle U_{lj}^{+J}(r)\rangle+\tfrac{1}{2}\sum_{\lambda(J)}\frac{\Gamma_{n\lambda}^{lj}}{E_\lambda-E-\frac{1}{2}i\Gamma_\lambda}N_{lj}(r)\ , \qquad (1)$$

$$N_{lj}(r)=\frac{\mathrm{Im}\langle U_{lj}^{+J}(r)\rangle}{\mathrm{Im}\langle K_{lj}^{J}\rangle}\ ,$$

to a bound single-particle orbit in the final state

$$\Psi_f=\sqrt{S_f}\,\frac{U_{l_fj_f}(r)}{r}\Phi_{l_fj_f}^{J_fM_f}\ . \qquad (2)$$

TABLE I. Comparison between the calculated and measured partial capture cross sections of ^{12}C, as well as relevant data at low neutron energies. $\sigma(n,\gamma_0)$, $\sigma(n,\gamma_1)$, $\sigma(n,\gamma_2)$, and $\sigma(n,\gamma_3)$ are the partial capture cross sections feeding the ground state (0.0 MeV, $\frac{1}{2}^-$), the first excited state (3.09 MeV, $\frac{1}{2}^+$), the second excited state (3.68 MeV, $\frac{3}{2}^-$), and the third excited state (3.85 MeV, $\frac{5}{2}^+$) in ^{13}C, respectively. $\sigma(n,\gamma_i)^{\mathrm{ch}}$ is the calculated channel-capture cross section. $\sigma(n,\gamma)^{\mathrm{st}}$ is the calculated total compound-nucleus capture cross section. $\sigma(n,n)$ is the neutron elastic-scattering cross section.

Cross sections and incident energy	Measured [Ref.]	Calculated	
$\sigma(n,\gamma_0)$ thermal energy (mb)	2.38 ± 0.05 [2]	$\sigma(n,\gamma_0)^{\mathrm{ch}}$	2.64
		$\sigma(n,\gamma_0)^{\mathrm{st}}$	0.30
$\sigma(n,\gamma_0)$ 30 keV (μb)	3.3 ± 0.9 [1]	$\sigma(n,\gamma_0)^{\mathrm{ch}}$	2.37
		$\sigma(n,\gamma)^{\mathrm{st}}$	0.26
$\sigma(n,\gamma_1)$ 30 keV (μb)	9.6 ± 1.3 [1]	$\sigma(n,\gamma_1)^{\mathrm{ch}}$	11.5
		$\sigma(n,\gamma)^{\mathrm{st}}$	0.26
$\sigma(n,\gamma_2)$ thermal energy (mb)	1.14 ± 0.02 [2]	$\sigma(n,\gamma_2)^{\mathrm{ch}}$	1.05
$\sigma(n,\gamma_2)$ 30 keV (μb)	1.7 ± 0.8 [1]	$\sigma(n,\gamma_2)^{\mathrm{ch}}$	0.83
$\sigma(n,\gamma_3)$ 30 keV (μb)	2.2 ± 1.1 [1]	$\sigma(n,\gamma_3)^{\mathrm{ch}}$	1.56
$\sigma(n,n)$ thermal energy (b)	4.75 [3]		5.05
$\sigma(n,n)$ 30 keV (b)	4.6 [3]		4.46

In this process, the target core keeps in its ground state as a spectator without disturbance. In Eq. (1), Re and Im designate real and imaginary parts, $\langle U_{lj}^{+J}(r)\rangle$ is the optical-model scattering wave function, $\langle K_{lj}^{J}\rangle$ is the optical-model reactance matrix element, λ refers to a nearby resonance with resonance parameters of E_λ, Γ_λ, and $\Gamma_{n\lambda}$. The function $N_{lj}(r)$ has the asymptotic form of $-kr\eta_l(kr)$ in the region outside the nuclear interaction, where $\eta_l(kr)$ is a spherical Neumann function. The first term in Eq. (1) is usually called the potential-scattering wave, corresponding to the potential capture, whereas the second term contains the contribution from the nearby resonances, and is related to the valence capture. In Eq. (2), S_f is the (d,p) spectroscopic factor, $U_{l_fj_f}(r)$ is the radial wave function of a single particle in the final state, $\Phi_{l_fj_fI}^{J_fM_f}$ is the channel wave function consisting of the intrinsic ground-state wave function of the target nucleus coupled to the neutron angular-momentum wave function to give total spin J_f and projection M_f.

Then the channel neutron radiative capture cross section from a scattering state (lj) to a final state f is [7]

$$\sigma_{lj,f}^{\rm ch}=\frac{4}{3}\frac{k_\gamma^3}{\hbar v}\frac{\pi}{k^2}\sum_J\frac{2J+1}{2(2I+1)}\langle ljJ||D_I||l_fj_fJ_f\rangle \times(2J_f+1)S_f\bar{e}^{\,2}\frac{4}{|1-i\langle K_{lj}^J\rangle|^2} \times\left|\int_R^\infty rU_{lj}^{+J}(r)U_{l_fj_f}(r)dr\right|^2, \tag{3}$$

where k and v are the neutron wave number and velocity, k_γ is the photon wave number, and $\bar{e}=-(Z/A)e$ is the neutron effective charge for $E1$ transition. The geometrical factor

$$\langle ljJ||D_I||l_fj_fJ_f\rangle=(2l+1)(2j+1)(2j_f+1)[C_{l010}^{l_f0}W(ljl_fj_f;\tfrac{1}{2}1)W(jJj_fJ_f;I1)]^2 \tag{4}$$

is the reduced matrix element of spin-angular part. The reader is referred to the original articles [4,7] for the detailed nomenclature. In the case of the target ^{12}C, one has $I=0$, and hence $j=J$, $j_f=J_f$, then Eq. (3) may be simplified as

$$\sigma_{lj,f}^{\rm ch}=\frac{16}{3}\frac{k_\gamma^3}{\hbar v}\frac{\pi}{k^2}\frac{2j+1}{2}(2l+1)(2j_f+1) \times[C_{l010}^{l_f0}W(ljl_fj_f,\tfrac{1}{2}1)]^2 \times S_f\bar{e}^{\,2}\frac{1}{|1-i\langle K_{lj}^j\rangle|^2} \times\left|\int_R^\infty rU_{lj}^{+j}(r)U_{l_fj_f}(r)dr\right|^2. \tag{5}$$

The optical-model potential used in this paper is of the same form as Ref. [4]: $R=r_0A^{1/3}$, $V_R=44.8$ MeV, $W=9.1$ MeV, $V_s=6.2$ MeV, $a=0.75$ fm, $r_0=1.25$ fm. This set of parameters is confirmed in reproducing the thermal neutron capture cross section feeding the ground state of ^{13}C [4], as well as the neutron-scattering cross sections in the energy region from thermal to 30 keV, as shown in Table I. In addition, the real part of the same potential is able to keep the binding energy of the single-particle $1p_{1/2}$ neutron orbit in ^{13}C at the experimental value, 4.95 MeV. It should be pointed out that, by using this set of parameters, the single-particle $2s_{1/2}$ and $1d_{5/2}$ orbits are unbound, and the $1p_{3/2}$ orbit is too deeply bound in comparison with the physical state. Thus, as we calculate the transitions to those real physical states in ^{13}C (3.09 MeV, $\frac{1}{2}^+$), (3.68 MeV, $\frac{3}{2}^-$), and (3.85 MeV, $\frac{5}{2}^+$), we must use an approximate wave function for each physical bound state, which is calculated with the adjusted parameters to reproduce the real binding energy of that state. For example, as we calculate the channel-capture cross sections to the first excited state (3.09 MeV, $\frac{1}{2}^+$), the parameters, $V_R=49.3$ MeV and $r_0=1.38$ fm, are used to obtain the wave function of the bound single-particle $2s_{1/2}$ orbit with binding energy of 1.90 MeV. The parameters for resonances at positive energies needed in Eq. (1) are taken from Ref. [8]. There are also four resonances at negative energies, which should be taken into account in calculating the scattering wave functions at the energy region concerned. Table II lists the related parameters for those resonances. The spectroscopic factors are taken from Refs. [8] and [9], and the reduced neutron widths are deduced from those factors [8].

Based upon the model presented above, we calculate

TABLE II. Parameters for negative resonances in the ^{12}C$(n,\gamma)^{13}$C reaction.

E_λ (MeV)	l	J	Γ_γ (eV)	$g\Gamma_n^{0b}$ (eV)
−1.183	2	$\frac{5}{2}$	0.5[a]	3416.0
−1.367	1	$\frac{3}{2}$	0.5[a]	207.0
−2.020	0	$\frac{1}{2}$	0.43	1200.0
−5.338	1	$\frac{1}{2}$	0.0	595.0

[a] Assigned.

[b] Deduced from the evaluated spectroscopic factors [8,9].

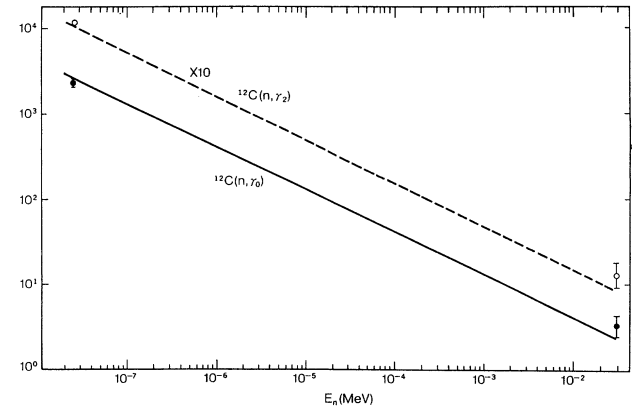

FIG. 1. Comparison between the calculated and measured partial capture cross sections of ^{12}C at low neutron energies. The solid curve is the calculated channel-capture cross sections feeding the ground state in ^{13}C (0.0 MeV, $\frac{1}{2}^-$). The measured data are shown by the solid circles. The dashed curve is the channel-capture cross sections to the second excited state in ^{13}C (3.68 MeV, $\frac{3}{2}^-$), and the related measured data are represented by the hollow circles.

the partial channel-capture cross sections feeding the first four bound states, the total compound-nucleus capture cross sections, as well as the neutron-scattering cross sections at neutron energies from thermal to 30 keV. The results are shown in Table I and in Figs. 1 and 2, along with the available measured data. Our main results and conclusions may be summarized as follows.

(1) The measured partial capture cross sections of ^{12}C at thermal energy and 30 keV are well understood in the framework of the channel-capture model for the $E1$ transition. The optical potential used in the calculations can also reproduce the neutron-scattering data at the energy region. The compound-nucleus capture cross sections are negligibly small at the energies concerned.

(2) The radiative capture transitions feeding the ground state in ^{13}C (0.0 MeV, $\frac{1}{2}^-$) are governed by the channel capture from the s-wave scattering state to the bound single-particle $1p_{1/2}$ orbit. A comparison is shown in Fig. 1. The destructive interference between the potential-scattering wave and the resonance-scattering wave keeps to work as the neutron energy varies from thermal to 30 keV. Therefore, the channel-capture cross section maintains much lower than the corresponding potential-capture cross section in this energy region. Figure 3 gives the radial integrands for both the potential capture $[r\,\mathrm{Re}\langle U^{+1/2}_{0,1/2}(r)\rangle U_{1,1/2}(r)]$ and the channel capture $[r\,\mathrm{Re}U^{+1/2}_{0,1/2}(r)U_{1,1/2}(r)]$ at 30 keV. The nearby negative s-wave resonance at -1.92 MeV plays a major role in causing the drastic cancellation for the radial integral of channel capture. The magnitude of this partial capture cross section follows the $1/v$ law quite well with neutron energy.

(3) The measured partial capture cross section feeding the first excited state in ^{13}C (3.09 MeV, $\frac{1}{2}^+$) can be attributed to the channel capture from the p-wave scattering state to the bound single-particle $2s_{1/2}$ orbit. Figure 2 plots a comparison of the calculated channel-capture cross sections with measured data. In this calculation, an approximate single-particle wave function obtained with modified potential parameters is needed for the physical final state. The contribution from the $p_{3/2}$-wave scattering is almost twice of that from the $p_{1/2}$-wave scattering. In contrast to the transition to the ground state, the resonance contribution is negligibly small. This is because the nearby $p_{3/2}$ negative resonance has a small reduced neutron width ($S_f=0.1$), and the nearby $p_{1/2}$ resonance,

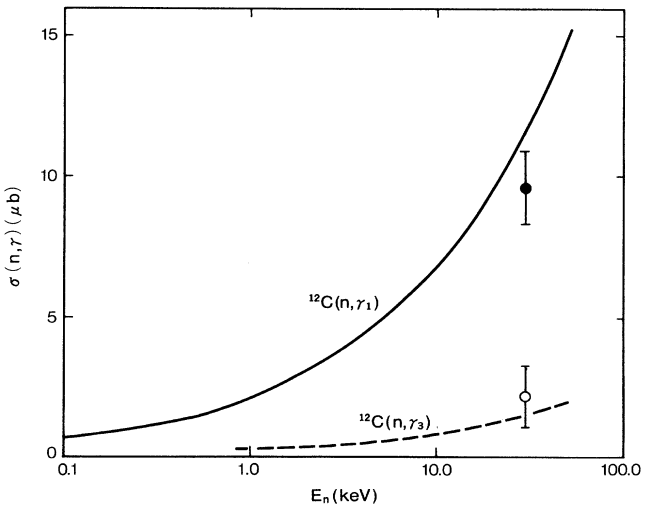

FIG. 2. The same convention as in Fig. 1, but for the transitions feeding the first excited state (3.09 MeV, $\frac{1}{2}^+$: solid curve and solid circle), and the third excited state (3.85 MeV, $\frac{5}{2}^+$: dashed curve and hollow circle) in ^{13}C.

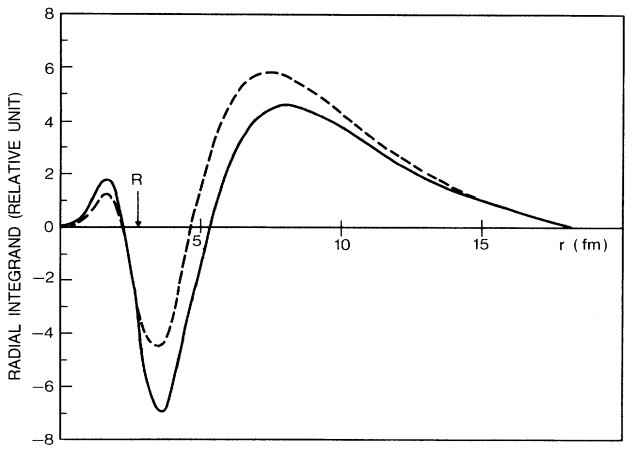

FIG. 3. Radial integrands for radiative capture of a scattering s-wave neutron into the bound $1p_{1/2}$ orbit in ^{12}C at 30 keV. The dashed line is the integrand for potential capture, whereas the solid line is for channel capture.

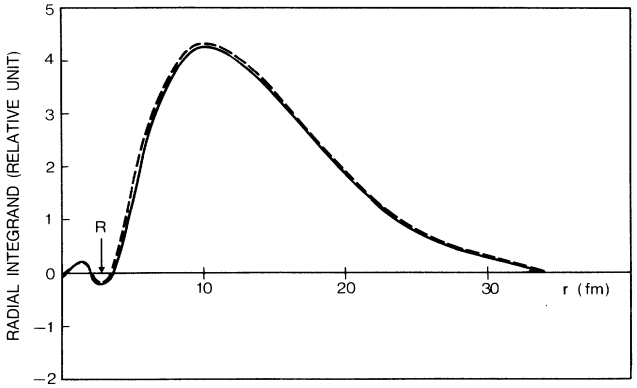

FIG. 4. The same convention as in Fig. 3, but for radiative capture of a scattering $p_{3/2}$-wave neutron into the bound $2s_{1/2}$ orbit.

the ground state in ^{13}C, is too far away in the energy space (−4.95 MeV) to make a significant contribution. Thus, the channel-capture cross section is almost the same as the potential-capture cross section. Figure 4 shows the radial integrands for both the potential capture $[r\,\mathrm{Re}<U^{+3/2}_{1,3/2}(r)>U_{0,1/2}(r)]$ and the channel capture $[r\,\mathrm{Re}U^{+3/2}_{1,3/2}(r)U_{0,1/2}(r)]$ at 30 keV. It can be seen that there is no notable difference between the two processes.

(4) The partial capture cross sections to the second excited state in ^{13}C (3.68 MeV, $\frac{3}{2}^-$) mainly result from the channel capture of the scattering s-wave neutron into the bound single-particle $1p_{3/2}$ orbit. The results are displayed in Fig. 1. A destructive interference, which is similar to that for the ground-state transition, is also observed, but with a relatively weak effect: the channel-capture cross section is about half of the potential-capture cross section. The channel-capture contribution from the d wave is negligibly small even at 30 keV.

(5) Figure 2 also contains a plot for the radiative transition feeding the third excited state in ^{13}C (3.85 MeV, $\frac{5}{2}^+$), which stems chiefly from the channel capture of the scattering $p_{3/2}$-wave neutron into the bound single-particle $1d_{5/2}$ orbit. Analogous to the transition to the first excited state, no obvious destructive interference between the potential-scattering wave and resonance-scattering wave appears in this process.

Y.-K. Ho is grateful to Professor H. Kitazawa and Professor M. Igashira for their kind hospitality during the short stay at the Tokyo Institute of Technology.

*Permanent address: Nuclear Science Department, Fudan University, Shanghai, China.

[1] Y. Nagai, M. Igashira, K. Takeda, N. Mukai, S. Motoyama, F. Uesawa, H. Kitazawa, and T. Fukuda, Astrophys. J. **372**, 68 (1991).

[2] M. A. Lone, in *Proceedings of the Fourth International Symposium on Neutron Capture Gamma-Ray Spectroscopy and Related Topics, Grenoble, 1981,* Institute of Phys. Conf. Series No. 62, edited by T. von Egidy, F. Gönnenwein, and B. Maier (Institute of Physics, Bristol, U.K., 1981), p. 383.

[3] V. McLane, C. L. Dunford, and P. F. Rose, *Neutron Cross Sections* (Academic, New York, 1988), Vol. 2.

[4] Y. K. Ho and M. A. Lone, Nucl. Phys. **A406**, 18 (1983).

[5] A. M. Lane and J. E. Lynn, Nucl. Phys. **17**, 563 (1960).

[6] S. Raman, R. F. Carlton, J. C. Wells, E. T. Jurney, and J. E. Lynn, Phys. Rev. C **32**, 18 (1985).

[7] Y. K. Ho and M. A. Lone, Nucl. Phys. **A406**, 1 (1983).

[8] S. F. Mughabghab, M. Divadeenam, and N. E. Holdon, *Neutron Cross Sections* (Academic, New York, 1981), Vol. 1.

[9] F. Ajzenberg-Selove, Nucl. Phys. **A449**, 1 (1986).